



## A binary gas transport model Improves the prediction of mass transfer in freeze drying

Ioan-Cristian Trelea, Fernanda Fonseca, Stéphanie Passot, Denis Flick

### ► To cite this version:

Ioan-Cristian Trelea, Fernanda Fonseca, Stéphanie Passot, Denis Flick. A binary gas transport model Improves the prediction of mass transfer in freeze drying. Drying Technology, 2015, 33 (15-16), pp.1849-1858. 10.1080/07373937.2015.1040025 . hal-01269386

HAL Id: hal-01269386

<https://hal.science/hal-01269386>

Submitted on 11 Jul 2017

**HAL** is a multi-disciplinary open access archive for the deposit and dissemination of scientific research documents, whether they are published or not. The documents may come from teaching and research institutions in France or abroad, or from public or private research centers.

L'archive ouverte pluridisciplinaire **HAL**, est destinée au dépôt et à la diffusion de documents scientifiques de niveau recherche, publiés ou non, émanant des établissements d'enseignement et de recherche français ou étrangers, des laboratoires publics ou privés.

## 1 Title:

## **2 A binary gas transport model improves the prediction of mass**

## **3 transfer in freeze-drying**

4

5 Short title: Binary gas transport model in freeze-drying

6

7     Ioan Cristian Trelea<sup>1,2\*</sup>, Fernanda Fonseca<sup>2,1</sup>, Stéphanie Passot<sup>1,2</sup>, Denis Flick<sup>3,4</sup>

8

<sup>1</sup>*AgroParisTech, UMR782 Génie et Microbiologie des Procédés Alimentaires,*

11 *1 av. Lucien Brétignières, F-78850 Thiverval-Grignon, France*

<sup>4</sup>INRA, UMR1145 Ingénierie Procédés Aliments  
1 av. des Olympiades, F-91300 Massy, France

<sup>19</sup>\*Corresponding author. Tel.: +33 1 30 81 54 00. E-mail: [christian.taylor@conseilrecherche.fr](mailto:christian.taylor@conseilrecherche.fr).

20

Monitoring partial vapor pressure in the freeze-drying chamber is a cheap, global and non-intrusive way to assess the end of the primary drying stage. Most existing dynamic freeze-drying models which predict this partial pressure describe mass transfer between the product and the condenser via a mass transfer resistance or a mass transfer coefficient. Experimental evidence suggests that such models can be significantly in error for some

values of the sublimation flux, leading to physically inconsistent predictions and possibly incorrect assessment of primary drying termination, with potential risk of product damage if moving to secondary drying and increasing shelf temperature while some ice is still present. Assuming a binary gas transport model for vapor and inert gas leads to improved and consistent predictions and explains the apparent variation of the mass transfer resistance with total pressure, shelf temperature and product sublimation area.

36

*Keywords:* lyophilization, dynamic model, mass transfer, convection, diffusion

39

40

## INTRODUCTION

42 Freeze-drying (lyophilization) is widely used for long term preservation of thermosensitive  
43 biological material and pharmaceuticals, such as proteins, vaccines, bacteria, mammalian cells  
44 and high quality food.<sup>[1, 2]</sup> It removes water or an organic solvent in a way that minimizes the  
45 modification of the molecular structure of the active ingredient and creates a porous matrix  
46 with high rehydration properties. Freeze-drying remains a costly process, however, and lot of  
47 research was devoted to its optimization, often based on mathematical modeling.<sup>[2, 3, 4, 5, 6, 7, 8,</sup>  
48 <sup>9, 10, 11, 12]</sup>

The process consists of three main steps: freezing, ice removal by sublimation (primary drying) and unfrozen water removal by desorption from the solid matrix (secondary drying). The primary drying stage is usually the most time and energy consuming part of a freeze-drying cycle. A lot of research has been devoted to the development of methods to precisely and consistently identify the end of the primary drying. Most of these methods rely on the monitoring of the vapor partial pressure in the freeze-drying chamber, either directly (moisture sensors such as aluminum oxide probes) and/or indirectly (Pirani gauge, mass spectrometer, Tunable Diode Laser Absorption Spectroscopy (TDLAS)).<sup>[13, 14]</sup> Moreover, abundant literature is available concerning modeling of primary freeze-drying for optimizing

58 this step of the process off line and also more recently in real time.<sup>[11, 12, 15]</sup> Models often  
59 predict the product temperature and the sublimation flux. The rate of solvent vapor removal  
60 from the product is usually described as being governed by three barriers or resistances:  
61 resistance of the dried-product layer, resistance of the containers (vials and stoppers), and  
62 resistance of the chamber to condenser pathway. Since the gas phase is mainly vapor during  
63 the primary drying and gradients of concentrations are small, true diffusion, or flow under the  
64 influence of a concentration gradient, is often considered of minor importance and models  
65 focus on bulk flow mechanisms.<sup>[16]</sup> The resistance of the dried product layer and of the  
66 containers has been studied both theoretically and experimentally by many groups. These  
67 studies present two limitations, however. Firstly, the chamber resistance is usually neglected  
68 because of measurement difficulties, or it is estimated by rather complex approaches  
69 involving Computational Fluid Dynamics (CFD) simulations.<sup>[17, 18, 19, 20]</sup> Secondly, the partial  
70 vapor pressure is usually not predicted but taken as fixed and equal to the total chamber  
71 pressure, despite its importance for real time optimization and freeze-drying control.<sup>[3, 10, 21, 22,</sup>  
72 <sup>23, 24]</sup>

73 Our group previously developed a one-dimensional heat and mass transfer model, which can  
74 accurately represent both the primary and secondary drying stages and the gradual transition  
75 between them.<sup>[9]</sup> When adapting it to other freeze-dryers and to bacterial suspensions,  
76 however, it turned out that the determined chamber resistance strongly varied with total  
77 pressure and shelf temperature. Moreover, for a sufficiently high sublimation flux, e.g.  
78 generated by a high shelf temperature at the beginning of the primary drying, the model can  
79 predict a partial vapor pressure higher than the total one, which is obviously incorrect.

80 In the present study the chamber resistance was experimentally determined and a model of  
81 mass transfer between the freeze-drying chamber and the condenser is proposed for the  
82 solvent vapor and inert gas pair. The model is based on the mass transfer theory in binary gas  
83 mixtures and includes bulk flow and mutual diffusion terms. This model improved the  
84 prediction of the chamber vapor pressure and of the primary drying termination. It also  
85 accounted for apparent variations of the effective mass transfer resistance with total pressure,  
86 shelf temperature and product sublimation area.

## MATERIALS AND METHODS

88 *Determination of the mass transfer resistance (vapor flow) of the chamber to condenser*  
89 *pathway*

90 Experiments were carried out on a LyoBeta special freeze-dryer (Telstar, Terrassa, Spain)  
91 equipped with 5 thermocouples, a capacitive manometer and a Pirani gauge. Purified water  
92 and bacterial cell suspensions were successively considered.

93 A stainless steel tray was filled with purified water to a thickness of 3 cm. The evaporative  
94 flow was determined using the gravimetric method. After freezing the water at -50°C (cooling  
95 rate of 0.6 °C/min), and sublimation time between 4 and 8 hours depending on the  
96 experimental conditions, the process was stopped and the tray was weighted to determine the  
97 amount of water removed and thus the evaporative flux ( $F_V$ , in kg s<sup>-1</sup>). The mass transfer  
98 coefficient ( $k_m$ , kg s<sup>-1</sup> Pa<sup>-1</sup>), or, equivalently, resistance of the chamber to condenser pathway  
99 ( $r_m$ , Pa s kg<sup>-1</sup>) was determined from Eq. 1:

100 Eq. 1

$$F_V = k_m (P_{V1} - P_{V2}) = \frac{P_{V1} - P_{V2}}{r_m}$$

101 with  $P_{V1}$ , the water vapor partial pressure just above the product (Pa), estimated from the ice  
102 temperature and  $P_{V2}$ , the water vapor partial pressure at the condenser (Pa), estimated from  
103 the condenser temperature.

104 The effect of three process variables on the effective mass resistance ( $r_m$ ) value was  
105 investigated: sublimation area (0.033, 0.074 and 0.15 m<sup>2</sup>), chamber pressure (10, 20, 40 and  
106 60 Pa) and shelf temperature (-15, 0 and 15°C).

107 *Freeze-drying experiments with bacterial suspensions*

108 Lactic acid bacteria were produced by fermentation in controlled conditions of pH and  
109 temperature.<sup>[25]</sup> After concentration, the bacterial cells were re-suspended in a 1:2  
110 cells/protective medium ratio. The protective medium was composed of 200 g/L of sucrose  
111 and 0.15 M of NaCl. A stainless steel tray was filled with 450g of bacterial suspension and  
112 the following freeze-drying protocol was applied: freezing at -50°C (cooling rate of  
113 0.6°C/min); primary drying at -20, 0 or 25°C; secondary drying at 25°C for 8 hours. The total  
114 chamber pressure was controlled at either 20 or 60Pa. Thermocouples were placed at the  
115 bottom of the product in the centre of the tray.

116    *Estimation of partial vapor pressure from the Pirani gauge*

117    The reading of a Pirani gauge in a pure gas is proportional to the pressure of the gas and to the  
118    molecular heat conductivity of the gas.<sup>[26]</sup> The main gases present in the freeze-drying  
119    chamber are solvent vapor (usually water) and an inert gas such as nitrogen or air. Let

120    Eq. 2

$$\alpha = \frac{\lambda_V}{\lambda_N}$$

121    be the ratio of the molecular heat conductivities. This ratio is equal to 1.6 for the water vapor  
122    and nitrogen pair. If the Pirani gauge is calibrated with inert gas, nitrogen in the present case,  
123    then the reading in pure solvent vapor will be:

124    Eq. 3

$$P_V^P = \alpha P_V$$

125    In a gas mixture, the Pirani gauge will measure the sum of heat fluxes due to conduction in  
126    each gas. The reading will be:

127    Eq. 4

$$P^P = \alpha P_V + P_N$$

128    In contrast, the capacitive sensor will give the true total pressure:

129    Eq. 5

$$P_t = P_V + P_N$$

130    From these two readings, one can determine the partial pressures of vapor and inert gas:

131    Eq. 6

$$P_V = \frac{P^P - P_t}{\alpha - 1}$$

132    Eq. 7

$$P_N = \frac{\alpha P_t - P^P}{\alpha - 1}$$

133    *Numeric calculations*

134    Calculations were performed with Matlab<sup>TM</sup> 8 software (The MathWorks Inc., Natick, MA)  
135    equipped with the Statistics Toolbox and the Global Optimization Toolbox.

## 136                MASS TRANSFER MODELS BETWEEN CHAMBER AND CONDENSER

137    *Mass transfer resistance model*

138    In most previously developed freeze-drying models, the mass flux between the freeze-drying  
139    chamber containing the product (location 1) and the condenser (location 2) was either

140 ignored, considering the vapor pressure in the freeze-drying chamber as given,<sup>[3, 10, 21, 22, 23]</sup> or  
141 expressed via a mass transfer coefficient ( $k_m$ ) or, equivalently, via a mass transfer resistance  
142 ( $r_m$ ),<sup>[9, 12, 27, 28, 29]</sup> as given by Eq. 1.

143 Note that in Eq. 1 the mass flux is proportional to the partial vapor pressure difference  
144 between the two locations. Vapor pressure  $P_{V2}$  is usually fixed by the condenser temperature,  
145 while the mass flux  $F_V$  is mostly determined by the heat transfer flux from the temperature-  
146 controlled shelf to the product, i.e. by the shelf temperature and the product sublimation area.  
147 If the mass transfer resistance was constant, as it is usually assumed, then the partial vapor  
148 pressure in the chamber  $P_{V1}$  would result from Eq. 1. If the mass flux was high enough, due  
149 for example to high shelf temperature, a model based on Eq. 1 could even give a vapor  
150 pressure higher than the total chamber pressure, which is obviously impossible. A more  
151 consistent mass transfer model is developed in the next section.

152 *Binary gas transport model*

153 Consider a mixture of two gases at low pressure; in the case of freeze-drying these gases  
154 would be solvent vapor, usually water, released from the product and captured by the  
155 condenser and the inert gas, usually nitrogen, used to control the total chamber pressure. To  
156 determine the relevant mass transport theory, the Knudsen number, defined as the ratio of the  
157 free mean path of the molecules and the characteristic dimension of the system, was  
158 estimated. In the considered conditions, the free mean path is of order of 0.5mm at 20Pa,  
159 while the typical diameter of the chamber to condenser duct is 100mm. Knudsen diffusion can  
160 thus be safely neglected for the chamber to condenser pathway considered here, since  
161  $K_n \approx 5 \times 10^{-3}$ . Note that this is usually not the case in the porous product layer where the pore  
162 size can be much less than 0.5mm, but mass transport in the porous layer is out of the scope  
163 of the present study.

164 The classical theory of binary diffusion in gases states that the molar flux density of solvent  
165 vapor, in stationary coordinates, is given by:<sup>[30]</sup>

166 Eq. 8 
$$N_V = x_V (N_V + N_N) - (c_V + c_N) D_{VN} \nabla x_V$$

167 where  $N_V$  and  $N_N$  are molar flux densities,  $c_V$  and  $c_N$  molar concentrations of vapor and  
168 nitrogen respectively,  $x_V$  is the molar fraction of vapor and  $D_{VN}$  is the mutual diffusion  
169 coefficient. The first term on the right-hand side of Eq. 8 results from the bulk motion of the  
170 fluid while the second one expresses the diffusion of vapor due to its molar fraction gradient.

171 Assuming pseudo-stationary conditions, compared to the duration of a freeze-drying cycle  
 172 which is of one or several days, and assuming insignificant leaks in the freeze-drying  
 173 chamber, the net inert gas flux is negligible compared to the vapor flux:

174 Eq. 9  $N_N \approx 0$

175 Usual variables in freeze-drying are mass fluxes instead of molar fluxes and partial pressures  
 176 instead of molar fractions and concentrations. Using the ideal gas law one gets:

177 Eq. 10  $x_V = \frac{P_V}{P_V + P_N} = \frac{P_V}{P_t}$

178 Eq. 11  $c_V + c_N = \frac{P_V + P_N}{RT} = \frac{P_t}{RT}$

179 Eq. 12  $f_V = M_V N_V$

180 With these substitutions, and assuming that the variation of total pressure between freeze-  
 181 drying chamber and condenser is small compared to the variation in vapour partial pressure,  
 182 Eq. 8 becomes:

183 Eq. 13  $f_V (P_t - P_V) = -\frac{M_V}{RT} P_t D_{VN} \nabla P_V$

184 To solve Eq. 13, it is assumed that the vapour flux between the product and the condenser is  
 185 essentially one-dimensional. This assumption is relatively sound for freeze-driers equipped  
 186 with a condenser separated from the main freeze-drying chamber by a pipe, as is the case in  
 187 the present study, but it is questionable when the product and the condenser are situated in the  
 188 same cavity. With this assumption, Eq. 13 can be integrated between the freeze-drying  
 189 chamber (location 1) and the condenser (location 2) giving:

190 Eq. 14  $F_V = A f_V = \frac{AM_V}{l_{eff} RT} P_t D_{VN} \ln \frac{P_t - P_{V2}}{P_t - P_{V1}}$

191 where  $F_V$  is the vapor mass flux, while  $A$  and  $l_{eff}$  are the diffusion cross-section area and  
 192 effective duct length respectively. The effective length accounts for the presence of inlet and  
 193 outlet sections, bends, valve and other elements that can introduce additional resistances.

194 The mutual gas diffusion coefficient  $D_{VN}$  is inversely proportional to the total pressure, thus  
195 the product  $P_t D_{VN}$  is constant.<sup>[30]</sup> For a given freeze-dryer geometry ( $l_{eff}$ ,  $A$ ) a constant  $\beta$  can  
196 be introduced:

197 Eq. 15

$$\beta = \frac{l_{eff} R}{AM_V P_t D_{VN}}$$

198 so that

199 Eq. 16

$$F_V = \frac{1}{\beta T} \ln \frac{P_t - P_{V2}}{P_t - P_{V1}}$$

200 The dependence of the mass flux on the partial vapor pressures given by Eq. 16 appears quite  
201 different from Eq. 1. It can be shown, however, using a first order Taylor series expansion of  
202 the logarithm function, that Eq. 1 is an approximation of Eq. 16 in the case when the vapor  
203 pressures are much less than the total pressure:

204 Eq. 17

$$\ln \frac{P_t - P_{V2}}{P_t - P_{V1}} \approx \frac{P_{V1} - P_{V2}}{P_t} \quad \text{if } P_{V1} \ll P_t \quad \text{and } P_{V2} \ll P_t$$

205 It should be noted, however, than in freeze-drying the condition  $P_{V1} \ll P_t$  is usually *not*  
206 satisfied as the gas in the freeze-drying chamber during primary drying is mostly solvent  
207 vapor. The approximation given by Eq. 17 is thus not expected to be valid. This can explain  
208 the mentioned inconsistency with Eq. 1 and the apparent variation of the effective mass  
209 transfer resistance with total pressure and mass flux, as further discussed below. For now,  
210 note that Eq. 16 can accommodate arbitrarily large vapor fluxes without  $P_{V1}$  exceeding  $P_t$ ,  
211 provided that the difference  $P_t - P_{V1}$  becomes small enough, while remaining positive.

212

## 213 RESULTS AND DISCUSSION

214 *Experimental determination of chamber to condenser mass transfer resistance*

215 Table 1 summarizes the experimental values of the mass transfer resistance of chamber to  
216 condenser pathway measured for various process conditions.

217 The effective mass transfer resistance appeared to increase when increasing chamber pressure,  
218 decreasing shelf temperature and decreasing sublimation area. The mass transfer resistance  
219 was thus inversely correlated with the sublimation flux. Increasing the sublimation rate

220 resulted in an apparent decrease of the effective mass transfer resistance of the chamber to  
221 condenser pathway. These observed variations support the idea that the mass transfer  
222 resistance is only an effective model parameter and a different perspective is needed to get a  
223 more physically meaningful description of the transfer phenomena. This is further discussed  
224 in the next sections.

225 *Prediction of partial vapor pressure in the chamber by the two modeling approaches:  
226 resistance vs. binary gas transport*

227 The predictions of the previously developed freeze-drying model,<sup>[9]</sup> adapted for bacterial  
228 suspension conditioned in trays, were compared to experimental measurements acquired in  
229 freeze-drying experiments performed as described in the “Materials and methods” section.  
230 Two versions of the model were tested, one based on a mass transfer resistance between the  
231 chamber and the condenser (Eq. 1) and the other based on the binary gas transport assumption  
232 (Eq. 16). Details of the existing model<sup>[9]</sup> adaptation to the new freeze-dryer, container and  
233 product, as well as implementation details of the new chamber-to-condenser mass transport  
234 model based on Eq. 16 are given in the Appendix. The model parameters (notably  $k_m$  and  $\beta$ )  
235 were determined by fitting the models to some of the experimental data obtained in bacterial  
236 suspension experiments (Appendix and Table 2)

237 An example of the predictions of the two versions of the model are shown in Figure 1, for two  
238 experiments performed at 0°C shelf temperature/60Pa chamber pressure and 25°C/20Pa,  
239 respectively. These are validation experiments not used for model parameter identification.  
240 Dotted lines represent calculations based on the mass transfer resistance model and solid lines  
241 correspond to the binary gas transport model.

242 The experiment at 0°C/60Pa (Figure 1, left panels) illustrates a situation where the prediction  
243 of the primary drying termination differs by about 2 hours between the considered models.  
244 The end of the primary drying was arbitrarily defined here as the moment when the  
245 sublimation flux (Figure 1C) decreased below 5% of its maximum value. The resistance  
246 model predicts the end of the primary drying at about 11h, in agreement with measured  
247 product temperature approaching the shelf temperature (Figure 1A), while the binary gas  
248 model predicts the end at about 13h, in agreement with the decrease of vapor pressure in the  
249 chamber (Figure 1B). Note that product temperature measurement is a local one, potentially  
250 disturbed by the presence of the probe, while partial vapor pressure measurement is a global  
251 one, representative of the whole product in the freeze-dryer. Vapor pressure should thus be

252 preferred to assess the end of the primary drying.<sup>[14]</sup> It is also non intrusive and usually more  
253 conservative, minimizing the risk of premature temperature increase and product damage, if  
254 some ice was still present when starting the secondary drying step.

255 The experiment at 25°C/20Pa (Figure 1, right panels) illustrates a situation where both models  
256 predict the same end point of the primary drying (11h), but the vapor pressure predicted by  
257 the resistance model is completely in error. Compared to the previously described experiment  
258 (0°C/60Pa), in this case the heat transfer resistance from the shelf to the product is higher due  
259 to lower chamber pressure (lower contribution of the gas conduction), but this is nearly  
260 compensated by a higher shelf temperature, leading to a similar heat flux. The net result is a  
261 similar primary drying time and sublimation flux (Figure 1C) for both experimental  
262 conditions. As expected from Eq. 1, a similar sublimation flux implies a similar vapor  
263 pressure calculated with the resistance model, around 50Pa in this case (Figure 1B), but this  
264 value is 2.5 times higher than the total pressure, which is obviously incorrect. In contrast, the  
265 binary gas model based on Eq. 16 consistently predicts a vapor pressure close to, but slightly  
266 less than the total one, as physically expected.

267 Both these examples suggest that the binary gas transport model should be preferred to the  
268 resistance model. Similar trends were observed in all performed experiments with bacterial  
269 suspensions (data not shown). The properties of the proposed binary gas transport model are  
270 further examined in the following sections.

271

### 272 *Effective mass transfer resistance of the chamber to condenser pathway*

273 Since Eq. 1 and Eq. 14 are two different ways of expressing the same vapor flux based on  
274 different physical assumptions, these equations can be used to define an effective mass  
275 transfer resistance of chamber to condenser pathway as:

276 Eq. 18

$$r_m = \frac{1}{k_m} = \frac{l_{eff} RT (P_{V1} - P_{V2})}{AM_V P_t D_{VN} \ln \frac{P_t - P_{V2}}{P_t - P_{V1}}} = \beta T \frac{P_{V1} - P_{V2}}{\ln \frac{P_t - P_{V2}}{P_t - P_{V1}}}$$

277 It readily appears from Eq. 18 that this resistance is not constant but is an effective model  
278 coefficient that depends on the actual values of the total and vapor pressure.

279 The effective mass transfer resistance given by Eq. 18 is plotted in Figure 2 (solid line) as a  
280 function of the vapor pressure near the product ( $P_{V1}$ ), for two different total pressures ( $P_t = 20$

281 and 60Pa) used in our experiments. The vapor pressure near the condenser was fixed to a low  
282 value  $P_{V2} = 0.055$  Pa, corresponding to a typical condenser temperature of  $-80^{\circ}\text{C}$ . For  
283 comparison, the value of  $r_m$  determined for the mass transfer resistance model in the same  
284 conditions is also given in Figure 2 (dotted line).

285 Firstly, Figure 2 indicates that the effective mass transfer resistance strongly increases with  
286 the total pressure. This was expected from the experimental data in Table 1 and confirms the  
287 usual practice of performing freeze-drying at low pressure to improve mass transfer.

288 Secondly, the effective mass transfer resistance predicted by the binary gas model approaches  
289 zero when the vapor pressure in the chamber approaches the total pressure. This was expected  
290 from the mathematical analysis of Eq. 18 and is consistent with the fact that partial vapor  
291 pressure in the chamber cannot exceed the total one, whatever the sublimation flux. Note that  
292 this is not the case with a constant mass transfer resistance, when the vapor pressure in the  
293 chamber can formally exceed the total pressure for a sufficiently high sublimation flux in Eq.  
294 1.

295 Finally, Figure 2 shows that the value of the mass transfer resistance determined using the  
296 resistance model based on Eq. 1 is situated between the bounds given by Eq. 18, as expected.  
297 The effective resistance given by the binary gas transport model is close to this value for  
298 vapor pressures very close to the total pressure. This means that the vapor pressure calculated  
299 by the binary gas model for the primary drying is most of the time very close to the total  
300 pressure, as observed in Figure 1 and well known from freeze-drying practice. This is further  
301 illustrated in the following section.

### 302 *Sublimation flux and predicted vapor pressure in the chamber*

303 In usual freeze-drying conditions the sublimation mass flux is the result of several process  
304 parameters (Table 1), such as total chamber pressure (that changes both heat and mass  
305 transfer), shelf temperature and sublimation interface area, etc. For the mass transfer  
306 resistance model given by Eq. 1, the predicted vapor pressure in the freeze-drying chamber  
307 varies linearly with the mass flux (dotted line in Figure 3) and can, as already mentioned,  
308 exceed the total pressure, for example in the case of a sufficiently high shelf temperature  
309 (Figure 1, right panels). In contrast, the vapor pressure predicted by the gas diffusion model  
310 given by Eq. 16 asymptotically tends towards the total pressure for high sublimation mass  
311 fluxes, which is physically consistent (solid lines in Figure 3). This also corroborates the well

312 known fact that gas composition in the freeze-drying chamber is dominated by vapor during  
313 most of the primary drying stage, when sublimation fluxes are high (approaching  $2 \times 10^{-5} \text{ kg s}^{-1}$   
314 in the considered experimental setting).

315 *Sublimation flux and effective mass transfer resistance of the chamber to condenser pathway*

316 Considering the effect of the sublimation mass flux in the binary gas transport model gives a  
317 common framework to understand the apparent variations of the effective mass transfer  
318 resistances observed in Table 1 for different shelf temperatures and sublimation interface  
319 areas. Increasing both these variables increases the sublimation flux and this, in turn, causes  
320 an apparent reduction of the effective mass transfer resistance (Figure 4). For sublimation  
321 fluxes approaching  $2 \times 10^{-5} \text{ kg s}^{-1}$ , representative of the primary drying in the considered  
322 experiments (Figure 1), the mass transfer resistance determined for the resistance model is  
323 intermediate between those calculated with the binary gas model for 20 and 60Pa total  
324 pressure. This reflects the compromise that the model fitting procedure finds to accommodate  
325 experiments performed at both these pressures, but the achieved compromise underestimates  
326 the vapor pressure at 60Pa and overestimates it at 20Pa, as already shown in Figure 1.

327 *The binary gas transport model needs a unique constant parameter*

328 As an additional difference between the two models, note that in the mass transfer resistance  
329 model the value of the resistance between the chamber and the condenser pathway is only an  
330 effective model parameter that appears to be a function of several process variables (Table 1):  
331 total pressure, shelf temperature and product sublimation area. Accounting for this would  
332 require varying the resistance in a tricky and ad-hoc manner. Considering a constant value of  
333 the mass transfer resistance ( $r_m = 2.78 \times 10^6 \text{ Pa s kg}^{-1}$  in our case) leads to poor predictions and  
334 inconsistencies, such as calculated partial vapor pressure in the chamber exceeding the total  
335 one (Figure 1 and Figure 3). On the contrary, binary gas diffusion theory states that the  
336 product  $P_D V_N$  is constant and therefore in the binary gas transport model the analogous  
337 parameter  $\beta$ , given by Eq. 15, is constant. All solid plots in Figures 1–4 were obtained with  
338 the same value of  $\beta = 2.66 \times 10^3 \text{ s kg}^{-1} \text{ K}^{-1}$ .

339 *In-process mass flux estimation and detection of the primary drying termination*

340 Eq. 16 could be used in principle for obtaining vapor flow rate estimations based on total and  
341 partial pressure measurements, and thus act as an in-process mass flow meter. In practice,

however, estimations of “high” vapor flow rates (i.e. when the partial vapor pressure approaches the total one) are expected to be inaccurate due to the vapor saturation of the chamber illustrated in Figure 3: a wide range of sublimation fluxes corresponds to almost identical partial vapor pressures, very close to the total chamber pressure. For example, with the considered values of the parameters (Appendix) at a total pressure of 60Pa, a vapor pressure of 59.99Pa corresponds to a sublimation flux of  $1.14 \times 10^{-5} \text{ kg s}^{-1}$ , while a vapor pressure of 58.99Pa corresponds to a sublimation flux of  $0.53 \times 10^{-5} \text{ kg s}^{-1}$ . In other words, an uncertainty of only 1Pa in the measurement of the vapor pressure would induce a factor 2 error on the flux value, which is clearly inappropriate for practical use.

On the contrary, Figure 3 suggests that the estimation of “low” vapor fluxes (i.e. when the partial vapor pressure is well below the total one) based on pressure measurements could be quite accurate. For example, vapor pressures of 30 and 29Pa correspond to vapor fluxes of  $0.091 \times 10^{-5} \text{ kg s}^{-1}$  and  $0.086 \times 10^{-5} \text{ kg s}^{-1}$  respectively; a measurement uncertainty of 1Pa would induce only about 5% error on the vapor flux.

Above considerations suggest that the proposed model is appropriate for a safe detection of the primary drying termination because a decrease of the vapor pressure well below the total one indicates a strong decrease of the sublimation flux. Continuing the above numerical examples, a vapor pressure in the chamber decreasing to the half of the total pressure corresponds to a factor 10 reduction of the sublimation flux. Of course, exact significance of “high” and “low” mass fluxes and the relevant decrease of vapor pressure depend on numerical values grouped in the parameter  $\beta$  defined by Eq. 15, and also involved in Eq. 16.

Finally, note that the proposed in-process flow estimation method based on total and partial pressure measurements in the chamber is complementary to the method described by Patel et al.<sup>[31]</sup>, based on differential pressure measurement between the chamber and the condenser. Indeed, the former works well for low sublimation fluxes while the latter is expected to be more accurate when the sublimation flux, and hence the measured pressure difference, are large.

## CONCLUSIONS

Results presented in this paper suggest that using one-dimensional mass transfer theory in binary gas mixtures to describe vapor transfer between the freeze-drying chamber and the condenser should be preferred to the mass transfer resistance approach. Advantages of the

binary gas transport model include: (i) prediction of the vapor pressure in the freeze-drying chamber closer to the experimental one, leading to more reliable prediction of the end of the primary drying; (ii) calculated values of the vapor pressure physically consistent with the total pressure, whatever the sublimation vapor flux; (iii) need to determine a single model parameter for a given freeze-dryer geometry, independent on the operating conditions (total pressure, shelf temperature, ice sublimation area).

The main drawback of the mass diffusion model is the non-linear dependence between the vapor flux and vapor pressure, which can somewhat complicate model simulations. Solution of non-linear differential and algebraic equation sets is already part of most freeze-drying models, however, and the additional difficulty introduced by the diffusion model is expected to be minor, as confirmed by the authors' experience.

The assumption of one-dimensional mass transfer between the freeze-drying chamber and the condenser could be questioned in the future, especially for freeze-dryers with the condenser situated in the freeze-drying chamber. The challenge would be to end up with a reasonably simple closed-form relationship between mass flux and pressure, in order to maintain the overall model minimalism and short simulation time.

## NOMENCLATURE

390	$c$	molar concentration	$\text{kmol m}^{-3}$
391	$f$	mass flux density	$\text{kg s}^{-1}\text{m}^{-2}$
392	$k$	mass transfer coefficient	$\text{kg s}^{-1}\text{Pa}^{-1}$
393	$l$	diffusion length	$\text{m}$
394	$r$	mass transfer resistance	$\text{Pa s kg}^{-1}$
395	$x$	molar fraction	$\text{kmol kmol}^{-1}$
396	$A$	diffusion cross-section area	$\text{m}^2$
397	$D$	mutual diffusion coefficient	$\text{m}^2 \text{s}^{-1}$
398	$F$	mass flux	$\text{kg s}^{-1}$
399	$K_n$	Knudsen number	—
400	$M$	molar mass	$\text{kg kmol}^{-1}$

401  $N$  molar flux density  $\text{kmol s}^{-1}\text{m}^{-2}$

402  $P$  pressure  $\text{Pa}$

403  $R$  ideal gas constant  $\text{J kmol}^{-1} \text{K}^{-1}$

404  $T$  absolute temperature  $\text{K}$

405 Greek letters

406  $\alpha$  heat conductivity ratio  $-$

407  $\beta$  mass transfer parameter  $\text{s kg}^{-1} \text{K}^{-1}$

408  $\lambda$  heat conductivity  $\text{Wm}^{-1} \text{K}^{-1}$

409 Subscripts

410 1 freeze-drying chamber, near product

411 2 condenser

412 3 ice sublimation front

413 4 product top

414  $eff$  effective

415  $m$  mass

416  $t$  total

417  $N$  inert gas, nitrogen

418  $V$  solvent vapor, water

419 Superscript

420  $P$  measured by Pirani gauge

421

422 **ACKNOWLEDGEMENT**

423 The research leading to these results has received funding from the European Community's  
424 Seventh Framework Programme (FP7/2007-2013) under grant agreement CAFE n° KBBE-  
425 212754.

426

427 APPENDIX: EMBEDDING THE BINARY GAS TRANSPORT EQUATION IN A  
428 COMPLETE FREEZE-DRYING MODEL

429 The binary gas transport equation proposed in this paper (Eq. 16) describes the mass flux  
430 between the freeze-drying chamber and the condenser, in replacement of the more classical  
431 equation involving a mass transfer resistance or a mass transfer coefficient (Eq. 1). Both  
432 equations were tested in conjunction with an existing freeze-drying model, described in full  
433 detail previously.<sup>[9]</sup>

434 In a first step, the parameters of the existing model<sup>[9]</sup> based on Eq. 1 were re-estimated to  
435 account for a different freeze-dryer (Lyobeta special freeze-dryer from Telstar, Terrassa,  
436 Spain, instead of SMH15 freeze dryer from Usifroid, Maurepas, France), a different container  
437 (metallic tray instead of glass vial) and a different product (lactic acid bacterial suspensions in  
438 sucrose medium instead of polyvinylpyrrolidone). Parameters related to the sorption isotherm  
439 and to the glass transition of the product were determined with the methodology described  
440 previously.<sup>[25]</sup> Parameters related to the heat and mass transfer in the freeze-dryer and in the  
441 product were estimated by fitting the product temperature and vapor pressure predicted by the  
442 model to experimental measurements. Four experiments were used simultaneously for model  
443 parameter estimation, performed in the following combinations of shelf temperature and total  
444 chamber pressure: -20°C/20Pa, -20°C/60Pa, 25°C/20Pa and 25°C/60Pa. A genetic  
445 optimization algorithm (Global Optimization Toolbox for Matlab, Natick, MA) was used for  
446 parameter identification. Since the considered optimization algorithm is stochastic, the  
447 parameter set with the best fit from 8 independent optimization runs was selected. Most  
448 optimization runs consistently converged to similar sets of parameters, usually within ±10%.  
449 Model parameters used in the present study are listed in Table 2.

450 In a second step, the original mass transfer equation between the chamber and the condenser  
451 (Eq. 1) was replaced by the newly proposed one (Eq. 16) and the parameter estimation  
452 procedure was repeated using the same data and the same algorithm. The estimated parameter  
453 values are also given in Table 2. As expected, the estimated values of the parameters are  
454 similar between the two models, with the exception of the parameter describing mass transfer  
455 between the freeze-drying chamber and the condenser ( $k_m$  for the resistance model and  $\beta$  for  
456 the binary gas transport model), which have different physical meanings.

457 Since the newly introduced equation is nonlinear and the vapor pressure in the chamber is  
458 unknown *a priori*, the sublimation flux cannot be determined explicitly as in the resistance

459 version of the model.<sup>[9]</sup> The vapor pressure in the chamber ( $P_{V1}$ ) was considered as an  
460 additional state variable and the corresponding mass balance equation in the freeze-drying  
461 chamber was added to the existing set of differential equations:

462 Eq. 19

$$\frac{M_V V_1}{RT} \cdot \frac{dP_{V1}}{dt} = F_{V31} - F_V$$

463 Here  $V_1$  is the freeze-drying chamber volume,  $F_V$  is the chamber to condenser vapor flux  
464 given by Eq. 16 and  $F_{V31}$  is the sublimation vapor flux between the ice sublimation front  
465 (location 3) and the freeze-drying chamber (location 1), given by:

466 Eq. 20

$$F_{V31} = \frac{1}{\frac{1}{k_{m34}} + \frac{1}{k_{m41}}} (P_{V3} - P_{V1})$$

467 where  $k_{m34}$  and  $k_{m41}$  are the mass transfer coefficients between the sublimation front and the  
468 product top (location 4), and between the product top and the chamber, respectively. Thus,  
469 both mass fluxes involved in Eq. 19 can be written explicitly in terms of known (fixed or  
470 state) variables ( $P_{V1}$ ,  $P_{V2}$ , and  $P_{V3}$ ).

471 Note that in the original freeze-drying model vapor accumulation in the freeze-drying  
472 chamber was neglected, based on a time scale analysis.<sup>[9]</sup> This is formally equivalent to  
473 setting the chamber volume  $V_1 \approx 0$  in Eq. 19, which would thus become an algebraic instead  
474 of a differential equation. This version of the model was also tested but not retained, due to  
475 occasional failures in solving the equation set during parameter identification. Observed  
476 difficulties are likely to be related to the specific differential-algebraic equations (DAE)  
477 solver available in Matlab (ode15s) which had numerical problems with some sets of  
478 parameters tested by the optimisation algorithm.

479

480

481

## REFERENCES

- 483 1. Tang, X.; Pikal, M.J. Design of freeze-drying processes for pharmaceuticals: practical  
484 advice. *Pharmaceutical Research*, 2004, 21(2), 191–200.
- 485 2. Sadikoglu, H.; Ozdemir, M.; Seker, M. Freeze-drying of pharmaceutical products:  
486 Research and development needs. *Drying Technology*, 2006, 24(7), 849–861.
- 487 3. Sadikoglu, H.; Liapis, A. Mathematical modelling of the primary and secondary drying  
488 stages of bulk solution freeze-drying in trays: parameter estimation and model  
489 discrimination by comparison of theoretical results with experimental data. *Drying  
490 Technology*, 1997, 15(3&4), 791–810.
- 491 4. Sadikoglu, H.; Liapis, A. I.; Crosser, O. K. Optimal control of the primary and secondary  
492 drying stages of bulk solution freeze drying in trays. *Drying Technology*, 1998, 16(3-5),  
493 399–431.
- 494 5. Sadikoglu, H.; Ozdemir, M.; Seker, M. Optimal control of the primary drying stage of  
495 freeze drying of solutions in vials using variational calculus. *Drying Technology*, 2003,  
496 21(7), 1307–1331.
- 497 6. Gan, K. H.; Bruttini, R.; Crosser, O. K.; Liapis, A. I. Heating policies during the primary  
498 and secondary drying stages of the lyophilization process in vials: effects of the  
499 arrangement of vials in clusters of square and hexagonal arrays on trays. *Drying  
500 Technology*, 2004, 22(7), 1539–1575.
- 501 7. Chouvinc, P.; Vessot, S.; Andrieu, J.; Vacus, P. Optimization of the freeze-drying cycle: a  
502 new model for pressure rise analysis. *Drying Technology*, 2004, 22(7), 1577–1601.
- 503 8. Boss, E. A.; Filho, R. M.; de Toledo, E. C. V. Freeze drying process: real time model and  
504 optimization. *Chemical Engineering and Processing*, 12 2004, 43(12), 1475–1485.
- 505 9. Trelea, I. C.; Passot, S.; Fonseca, F.; Marin, M. An interactive tool for freeze-drying cycle  
506 optimisation including quality criteria. *Drying Technology*, 2007, 25, 741–751.
- 507 10. Velardi, S. A. and Barresi, A. A. Development of simplified models for the freeze-  
508 drying process and investigation of the optimal operating conditions. *Chemical  
509 Engineering Research & Design*, 2008, 86(A1), 9–22.

- 510 11. Pisano, R.; Fissore, D.; Velardi, S. A.; Barresi, A. A. In-line optimization and control  
511 of an industrial freezedrying process for pharmaceuticals. *Journal of Pharmaceutical*  
512 *Sciences*, 2010, 99(11), 4691–4709.
- 513 12. Antelo, L. T.; Passot, S.; Fonseca, F.; Trelea, I. C.; Alonso, A. A. Toward optimal  
514 operation conditions of freeze-drying processes via a multilevel approach. *Drying*  
515 *Technology*, 2012, 30(13), 1432–1448.
- 516 13. Gieseler, H.; Kessler, W. J.; Finson, M.; Davis, S. J.; Mulhall, P. A.; Bons, V.; Debo,  
517 D. J.; Pikal, M. J. Evaluation of tunable diode laser absorption spectroscopy for in-process  
518 water vapor mass flux measurements during freeze drying. *Journal of Pharmaceutical*  
519 *Sciences*, 2007, 96(7), 1776–1793.
- 520 14. Patel, S. M.; Doen, T.; Pikal, M. J. Determination of end point of primary drying in  
521 freeze-drying process control. *AAPS Pharmaceutical Science and Technology*, 2010,  
522 11(1), 73–84.
- 523 15. Fissore, D.; Velardi, S. A.; Barresi, A. A. In-line control of a freeze-drying process in  
524 vials. *Drying Technology*, 2008, 26(6), 685–694.
- 525 16. Pikal, M. Heat and mass transfer in low-pressure gases: applications to freeze-drying.  
526 *Drugs and the Pharmaceutical Sciences*, 2000, 102, 611–686.
- 527 17. Alexeenko, A. A.; Ganguly, A.; Nail, S. L. Computational analysis of fluid dynamics  
528 in pharmaceutical freeze-drying. *Journal of Pharmaceutical Sciences*, 2009, 98(9), 3483–  
529 3494.
- 530 18. Rasetto, V.; Marchisio, D. L.; Fissore, D.; Barresi, A. A. On the use of a dual-scale  
531 model to improve understanding of a pharmaceutical freeze-drying process.  
532 *Pharmaceutical Technology*, 2010, 99(10), 4337–4350.
- 533 19. Ganguly, A. and Alexeenko, A. A. Modeling and measurements of water–vapor flow  
534 and icing at low pressures with application to pharmaceutical freeze-drying. *International*  
535 *Journal of Heat and Mass Transfer*, 2012, 55, 5503–5513.
- 536 20. Petitti, M.; Barresi, A.; Marchisio, D. L. Cfd modelling of condensers for freeze-  
537 drying processes. *Sadhana-Academy Proceedings in Engineering Sciences*, 2013, 38(6),  
538 1219–1239.

- 539 21. Mascarenhas, W. J.; Akay, H. U.; Pikal, M. J. A computational model for finite  
540 element analysis of the freeze-drying process. *Computer Methods in Applied Mechanics*  
541 and *Engineering*, 8/15 1997, 148(1-2), 105–124.
- 542 22. Sheehan, P. and Liapis, A. I. Modeling of the primary and secondary drying stages of  
543 the freeze drying of pharmaceutical products in vials: Numerical results obtained from the  
544 solution of a dynamic and spatially multi-dimensional lyophilization model for different  
545 operational policies. *Biotechnology and Bioengineering*, 1998, 60(6), 712–728.
- 546 23. Song, C. S.; Nam, J. H.; Kim, C. J.; Ro, S. T. A finite volume analysis of vacuum  
547 freeze drying processes of skim milk solution in trays and vials. *Drying Technology*, 2002,  
548 20(2), 283–305.
- 549 24. Hottot, A.; Peczalski, R.; Vessot, S.; Andrieu, J. Freeze-drying of pharmaceutical  
550 proteins in vials: modeling of freezing and sublimation steps. *Drying Technology*, 2006,  
551 24(5), 561–570.
- 552 25. Passot, S.; Cenard, S.; Douania, I.; Trelea, I. C.; Fonseca, F. Critical water activity and  
553 amorphous state for optimal preservation of lyophilized lactic acid bacteria. *Food*  
554 *Chemistry*, 2012, 132, 1699–1705.
- 555 26. Jennings, T. Lyophilization: Introduction and basic principles. Interpharm/CRC: Boca  
556 Raton, 1999.
- 557 27. George, J. P. and Datta, A. K. Development and validation of heat and mass transfer  
558 models for freeze-drying of vegetable slices. *Journal of Food Engineering*, 3 2002, 52(1),  
559 89–93.
- 560 28. Chouvinc, P.; Vessot, S.; Andrieu, J.; Vacus, P. Optimization of pharmaceuticals  
561 freeze-drying cycles: characterization of annealing effects by the pressure rise analysis  
562 method. In *Drying 2004 – Proceedings of the 14th International Drying Symposium (IDS*  
563 2004), São Paulo, Brazil, August 22-25, 2004; 359–365.
- 564 29. Hottot, A.; Vessot, S.; Andrieu, J. Determination of mass and heat transfer parameters  
565 during freeze-drying cycles of pharmaceutical products. *PDA Journal of Pharmaceutical*  
566 *Science and Technology*, 2005, 59(2), 138–153.
- 567 30. Bird, R.; Stewart, W.; Lighthfoot, E. *Transport phenomena*. Wiley: New York, 1960.

568 31. Patel, S. M.; Chaudhuri, S.; Pikal, M. J. Choked flow and importance of Mach I in  
569 freeze-drying process design. *Chemical Engineering Science*, 2010, 65, 5716–5727.  
570

571

572 Figure captions

573

574 Figure 1. Comparison between experimental measurements and simulations with the binary  
575 gas transport and resistance models, for two experiments with lactic acid bacteria  
576 suspensions (left panel 0°C/60Pa, right panel 25°C/20Pa). (A): Shelf and product  
577 temperatures, (B): Total and vapour pressures, (C): Sublimation fluxes. Bold: shelf  
578 temperature and total pressure, symbols: measurements, solid: binary gas model, dotted:  
579 resistance model, vertical line: end of primary drying.

580

581 Figure 2. Variation of the effective mass transfer resistance with the vapor and total pressure.  
582 Numeric values are for lactic acid bacteria suspension. Solid: binary gas model, bold: total  
583 pressure 60Pa, thin: total pressure 20Pa, dotted: resistance model.

584

585 Figure 3. Predicted vapor pressure as a function of the sublimation mass flux. Numeric values  
586 are for lactic acid bacteria suspension. Solid: binary gas transport model, bold: total  
587 pressure 60Pa, thin: total pressure 20Pa, dotted: resistance model.

588

589 Figure 4. Apparent variation of the effective mass transfer resistance of the chamber to  
590 condenser pathway as a function of the sublimation mass flux. Numeric values are for  
591 lactic acid bacteria suspension. Solid: binary gas transport model, bold: total pressure  
592 60Pa, thin: total pressure 20Pa, dotted: resistance model.

593

594

595

596 Table 1. Chamber to condenser mass transfer resistance measured with pure ice.

597

Total chamber pressure (Pa)	Shelf temperature (°C)	Sublimation interface area (m <sup>2</sup> )	Chamber to condenser resistance (10 <sup>6</sup> Pa s/kg)
10	0	0.074	0.65
20			1.29
40			2.64
60			3.72
40	-15 0 15	0.074	4.31 2.64 1.61
20	0	0.033 0.074 0.15	2.34 1.29 0.67

598

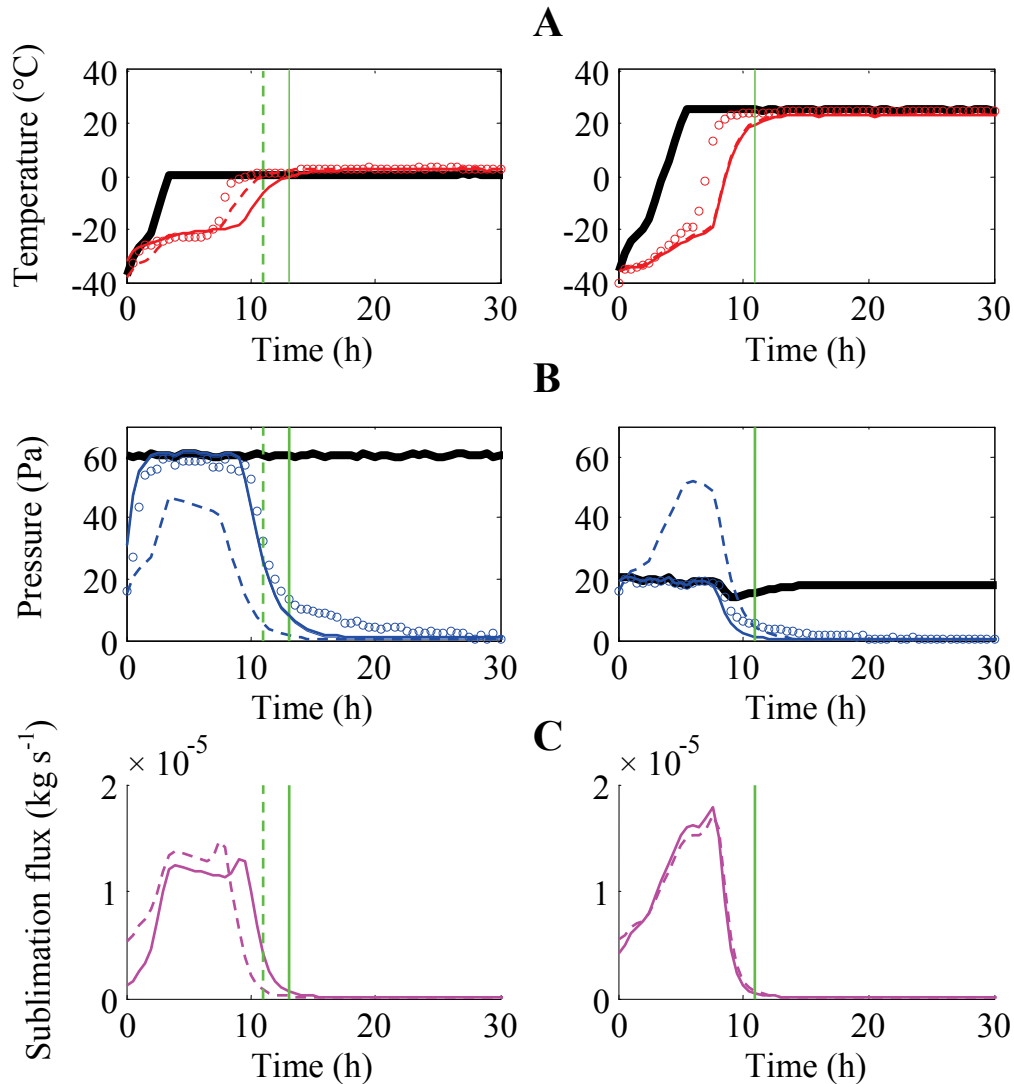
599

600 Table 2. Values of the freeze-drying model parameters

<i>Parameters defined by the experimental setup</i>		
Number of trays (-)	1	
Sublimation area ( $\text{m}^2$ )	0.0745	
Mass of dry product (kg)	0.0736	
Mass of ice (kg)	0.3763	
Product height in the tray (m)	0.0067	
Volume of the freeze-drying chamber ( $\text{m}^3$ )	0.202	
<i>Parameters specific for the product formulation, determined in separate experiments<sup>[25]</sup></i>		
Sorption isotherm, wet basis ( $\text{kg kg}^{-1}$ )	$0.3190a_w$ $(1 - 0.9827a_w)(1 + 6.3668a_w)$	
Characteristic desorption time (s)	10100	
Glass transition temperature of the frozen product ( $^\circ\text{C}$ )	-36	
Glass transition temperature of the perfectly dry product ( $^\circ\text{C}$ )	75.6	
Gordon-Taylor coefficient for glass transition temperature (-)	8.2	
<i>Heat and mass transfer parameters determined by model fitting</i>		
	<i>Mass transfer resistance model</i>	<i>Binary gas transport model</i>
Heat transfer coefficient by contact and radiation, between shelf and product bottom ( $\text{W m}^{-2} \text{K}^{-1}$ )	6.74	7.29
Heat transfer coefficient by gas conduction, between shelf and product bottom ( $\text{W m}^{-2} \text{K}^{-1} \text{Pa}^{-1}$ )	0.400	0.366
Heat conductivity between sublimation front and product top ( $\text{W m}^{-1} \text{K}^{-1}$ )	0.0957	0.0996
Heat transfer coefficient between product top and chamber walls ( $\text{W m}^{-2} \text{K}^{-1}$ )	3.79	3.03
Vapor conductivity between sublimation front and product top ( $\text{kg s}^{-1} \text{m}^{-1} \text{Pa}^{-1}$ )	$2.07 \times 10^{-8}$	$1.98 \times 10^{-8}$
Vapor transfer coefficient between product top and chamber ( $\text{kg s}^{-1} \text{m}^{-2} \text{Pa}^{-1}$ )	$8.12 \times 10^{-5}$	$3.68 \times 10^{-4}$
Vapor transfer coefficient between chamber and condenser $k_m$ ( $\text{kg s}^{-1} \text{Pa}^{-1}$ )	$3.60 \times 10^{-7}$	Not applicable
Vapor transfer parameter between chamber and condenser $\beta$ ( $\text{s kg}^{-1} \text{K}^{-1}$ )	Not applicable	$2.66 \times 10^3$
Residual frozen layer thickness for gradual transition between primary and secondary drying (m)	0.00173	0.00170
Effective chamber wall temperature ( $^\circ\text{C}$ )	15.3	13.9

601 Complete model equations and exact definitions of the model parameters are given in ref.<sup>[9]</sup>

602  
603



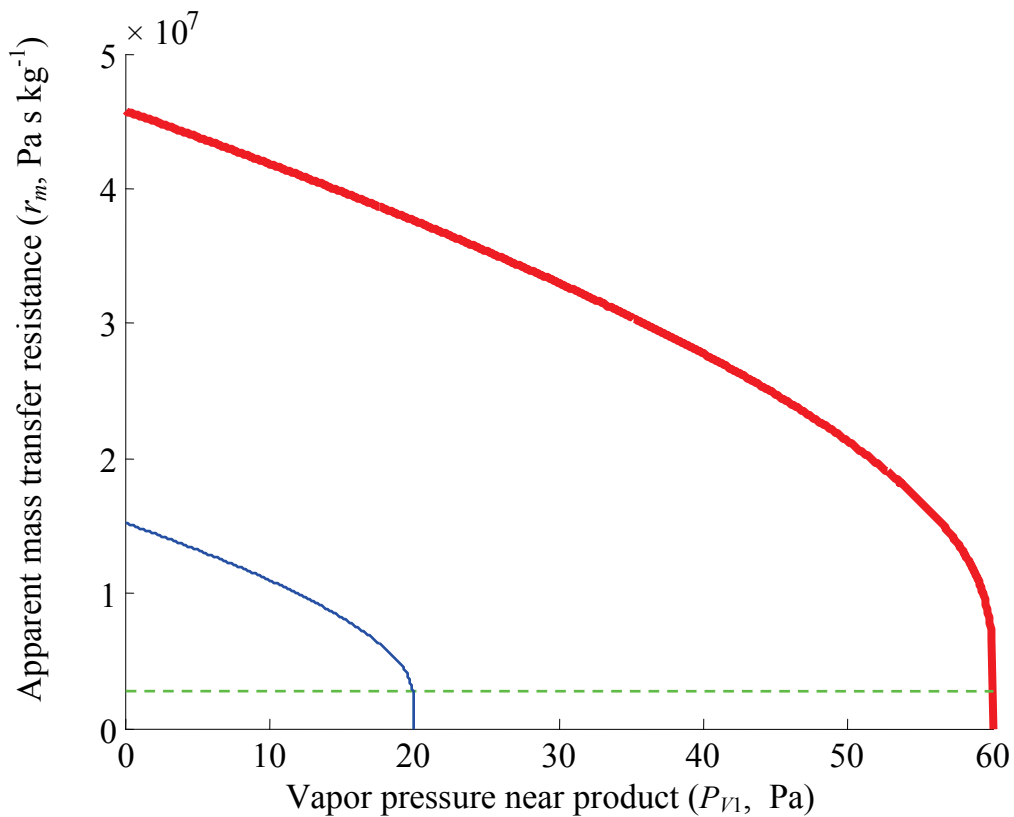
604  
605

606 Figure 1. Comparison between experimental measurements and simulations with the binary  
607 gas transport and resistance models, for two experiments with lactic acid bacteria suspensions  
608 (left panel 0°C/60Pa, right panel 25°C/20Pa). (A): Shelf and product temperatures, (B): Total  
609 and vapour pressures, (C): Sublimation fluxes. Bold: shelf temperature and total pressure,  
610 symbols: measurements, solid: binary gas model, dotted: resistance model, vertical line: end  
611 of primary drying.

612

613

614



615

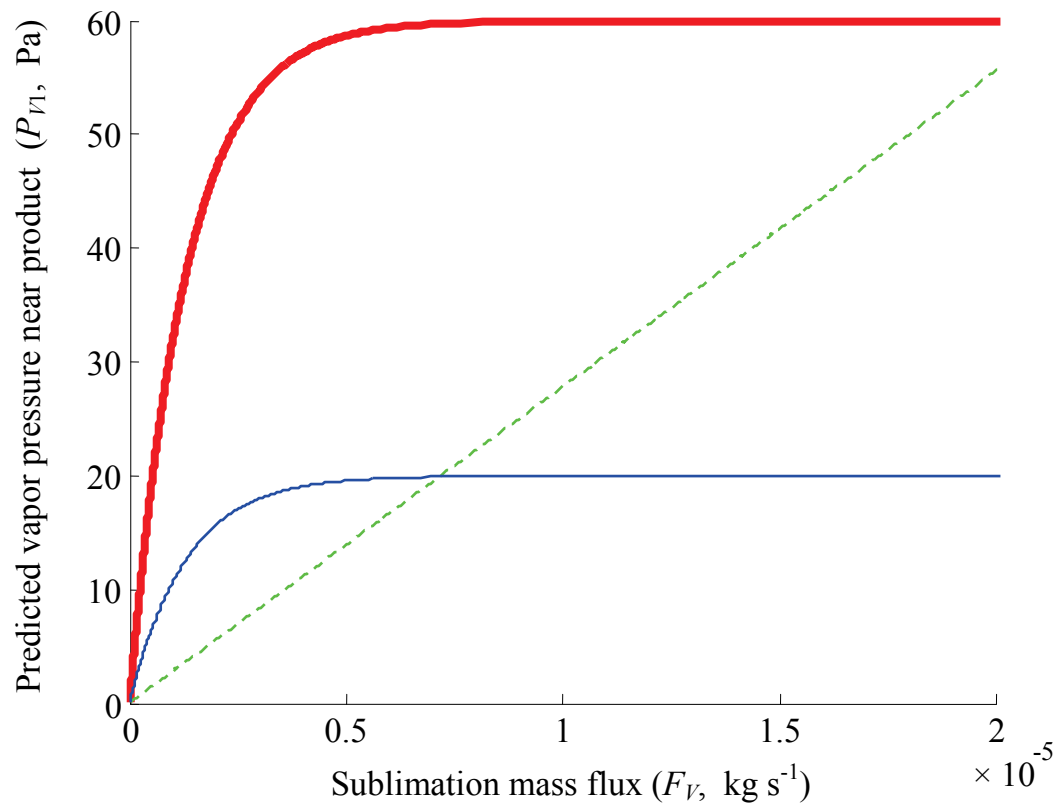
616

617 Figure 2. Variation of the effective mass transfer resistance with the vapor and total pressure.  
618 Numeric values are for lactic acid bacteria suspension. Solid: binary gas model, bold: total  
619 pressure 60Pa, thin: total pressure 20Pa, dotted: resistance model.

620

621

622



623

624

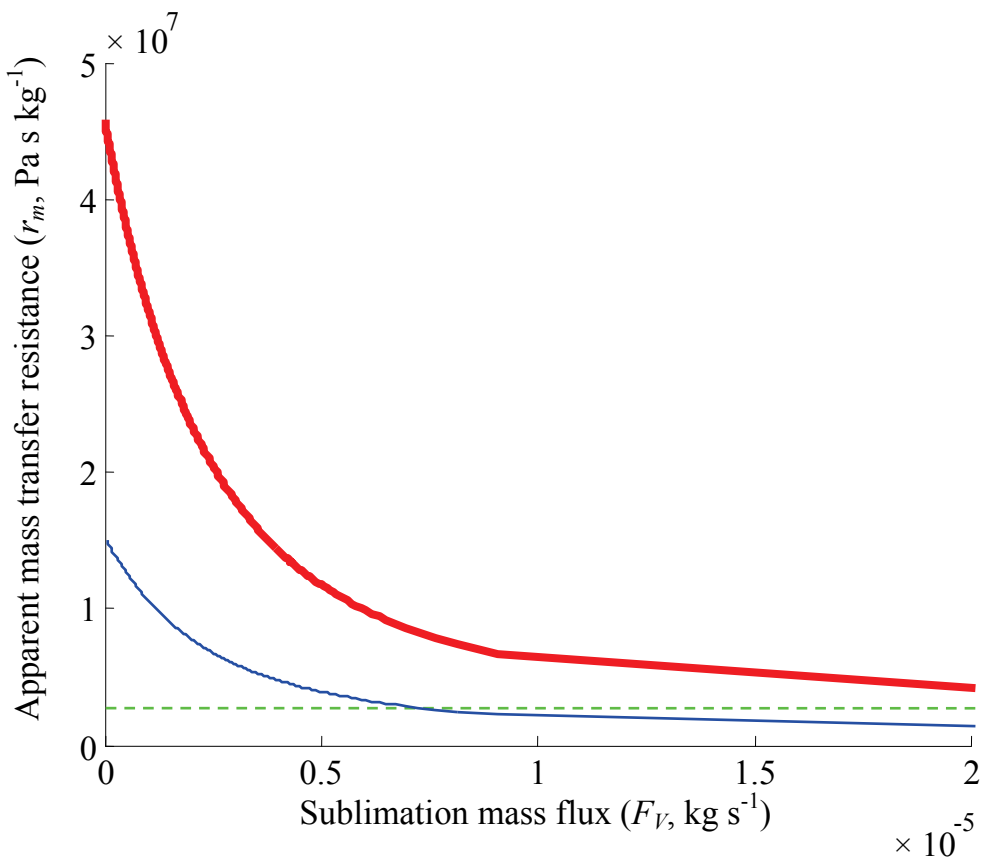
625 Figure 3. Predicted vapor pressure as a function of the sublimation mass flux. Numeric values  
626 are for lactic acid bacteria suspension. Solid: binary gas transport model, bold: total pressure  
627 60Pa, thin: total pressure 20Pa, dotted: resistance model.

628

629

630

631



632

633

634 Figure 4. Apparent variation of the effective mass transfer resistance of the chamber to  
635 condenser pathway as a function of the sublimation mass flux. Numeric values are for lactic  
636 acid bacteria suspension. Solid: binary gas transport model, bold: total pressure 60Pa, thin:  
637 total pressure 20Pa, dotted: resistance model.

638

639

640